공학석사 학위논문

Monte Carlo Perturbation Analysis of Isothermal Temperature Reactivity Coefficient in Light-Water Moderated Critical Assembly

몬테칼로 섭동법을 사용한 경수 감속 임계 집합체의 등온 반응도 계수 분석

2014년 8월

서울대학교 대학원

에너지시스템 공학부

전 병 규

Abstract

The isothermal temperature reactivity coefficient (ITRC) of the light water-moderated core with or without the D_2O tank in the Kyoto University Critical Assembly are analyzed by the Monte Carlo (MC) neutron transport analysis code, McCARD. Through the temperature changes of H_2O and D_2O, the effects of the coolant density changes in the moderator and reflector regions, and the microscopic cross section variations on ITRC are investigated by the sensitivity analyses by the MC adjoint-weighted perturbation method. Also, to obtain ITRC contributions of hydrogen and deuterium cross sections in thermal neutron energy region, a new perturbation technique for the thermal scattering library is presented. From results of MC perturbation analyses with help of the new technique, the ITRCs of the two core configurations are accurately estimated by competitions between a negative contribution of number density change of hydrogen in the moderator region and a positive contribution of the thermal scattering cross section change of hydrogen in the reflector region.

Keywords:

Isothermal Temperature Reactivity Coefficient

Kyoto University Critical Assembly

Monte Carlo Perturbation

McCARD

Student Number: 2012-23285

Contents

List of Tables

List of Figures

Chapter 1. Introduction

The temperature reactivity coefficient (TRC) in nuclear reactors is one of the most important reactor physics parameters to assess its inherent safety and maintain safety during operation. Sensitivities of the reactivity to region-wise and isotope-wise temperature changes may be useful in economically optimizing the core design. However, the TRC calculations have been considered difficult for research reactors, due to their complex geometry [1]. The continuous-energy Monte Carlo (MC) transport analysis can be useful for the TRC calculations by its high-fidelity modeling capability. However, the MC analysis requires huge computational time to obtain a reliable estimation of the small reactivity caused by a temperature change when the reactivity change is attained by subtracting two reactivity values estimated at different temperatures by the MC calculations.

1.1 Previous Researches

In order to overcome the weak point of the MC direct subtraction approach, L. B. Miller [2] earlier devised the temperature-derivative

estimator to calculate the Doppler coefficient of a fast breeder reactor from the MC neutron simulations. H. Rief [3] applied the correlated sampling (CS) and the differential operator sampling (DOS) methods to estimate the coolant temperature reactivity coefficient in a D_2O test reactor. For an accuracy enhancement, the CS and DOS methods augmented by the fission source perturbation [4] or the adjoint-weighting [5, 6] were successfully developed to estimate the reactivity change due to the density and microscopic cross section perturbation. An MC adjoint-weighted correlate sampling (AWCS) method for the Doppler coefficient estimation [7] was newly proposed to take into account of a perturbation of the transfer probability in the scattering kernel of free monatomic-gas models [8, 9] due to a temperature variation.

1.2 Objectives

The isothermal temperature reactivity coefficients (ITRCs) of the tank-type light water-moderated core (C-core) in the Kyoto University Critical Assembly (KUCA) [10] are analyzed experimentally and numerically by the Seoul National University MC code, McCARD [11], for its two configurations: with and without a D_2O tank immersed

in the core tank. The ITRC experiments were carried out to investigate the moderation and reflection effects of H_2O and D_2O, and to demonstrate a McCARD capability of the TRC estimation. The previous ITRC analyses [1, 12, 13] at the KUCA C-core had been conducted by the eigenvalue and perturbation calculations with the use of a diffusion code, CITATION [14] in the SRAC code system [15]. In current analyses, ITRC calculations are performed using MC approach to accurately represent the core geometry and continuous-energy microscopic cross section. Furthermore, detailed sensitivity can be calculated by the adjoint-weighted perturbation (AWP) methods [6, 7] in MC calculations. In order to produce the ITRC of the KUCA C-core by the AWP method, the perturbation of thermal scattering cross sections must be considered. However, it is known that perturbation calculation in thermal region is difficult since a scattering spectrum of thermal neutron varies to the temperature change.

This study aims to estimate the KUCA ITRC by the AWP methods to verify the capability of the AWP method for the ITRC estimation and the sensitivity analyses of the ITRC in the MC continuous-energy calculations. Especially, to overcome the difficulty of perturbation calculation in thermal region, the AWCS technique for the

stochastic mixing technique of cross section libraries [16] has been devised to estimate the reactivity change by the perturbation of thermal scattering cross sections due to the temperature changes. With the newly devised technique, the effect of thermal scattering library for the ITRC of thermal nuclear reactor can be estimated by the AWP method.

The ITRC experiments at the KUCA C-core with and without the D_2O tank is described in Chapter 2. In Chapter 3, the AWP method applied in this study is briefly presented and the CS approach for the stochastic mixing of the thermal scattering libraries (TSLs) is exhibited. Chapter 4 reveals the comparison between the measured and calculated excess reactivities with varying the system temperature. The sensitivities of the ITRC to the region-wise and isotope-wise changes are also shown.

Chapter 2. The KUCA ITRC Experiments

The Kyoto University Critical Assembly (KUCA) is a center for the research on reactor physics, organized and operated by the Kyoto University, Japan [10]. The experiments on the ITRC at the KUCA C-core with and without the D_2O tank immersed in the core tank were carried out with the variation of the system temperature in August 2012 and January 2013, respectively. The variation is considered important to investigate the moderation and reflection effects of H_2O and D_2O in the core.

2.1 The KUCA Facility

The KUCA is a multi-core type, which consists of two solid-moderated cores (A & B Cores) and one light-water moderated core (C-core). Users can select the most appropriate core for their experimental purposes [10]. One of the purposes of the KUCA is to validate codes through experiments and analysis. In accordance to this purpose, experiment results are utilized for verification of the MC AWP method, as the temperature coefficient estimator. The KUCA C-core is suitable

for the ITRC estimation of hydrogen and deuterium, since C-core uses the light-water as the coolant and D_2O tank can be installed in the core.

2.1.1 The KUCA C-Core Features

In the core tank with 2,000 mm in diameter and 2,000 mm in depth, two grid plates are equipped for setting fuel frames, control and safety rods, and detectors as shown in Fig. 2-1 [10]. A dump tank is placed under the core tank. The light water is pumped up into the core tank to supply the moderator and reflector during the reactor operation.

There are three types of fuel frame in the KUCA C-core. Each fuel frames has different sizes of pitch to change the water-to-uranium ratio of the core. In this experiment, the C35 type fuel frame was used. The C35 type fuel frame has the coolant channel of 1.99 mm, and a maximum of 40 fuel plates can be inserted corresponding to the critical mass.

The dimension of fuel plate is as follows: 600 mm in length, 62 mm in width, and 1.5 mm thick. The fuel plate is composed of highly enriched U-Al alloy as fuel meat and two 0.5 mm thick layers of aluminum.

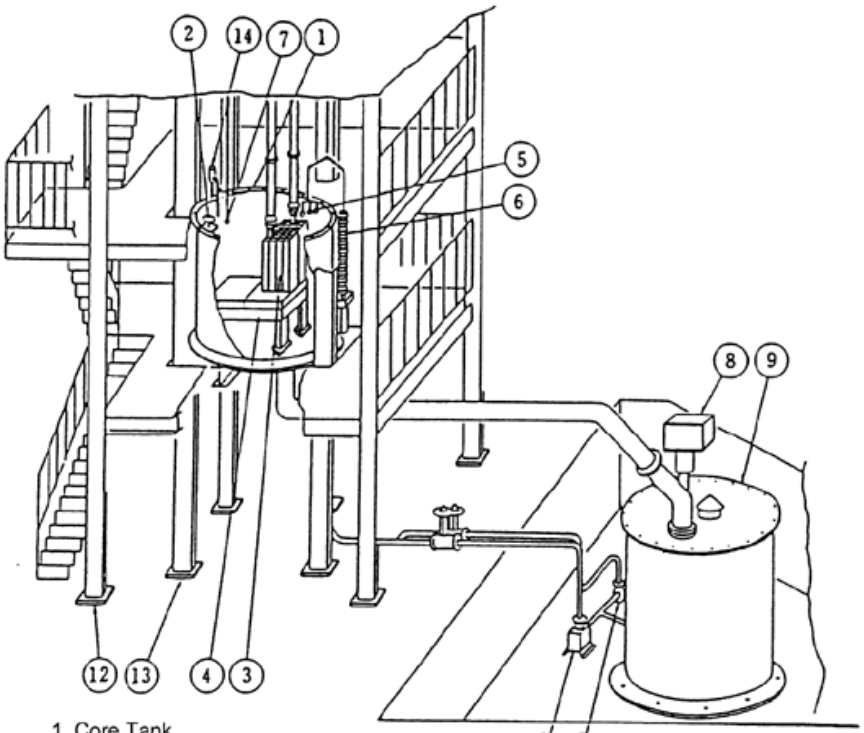

1. Core Tank
2. Handl for the core separation mechanism
3. Core assembly
4. Core separation mechanism
5. Float switch to detect the core over flow
6. Over flow tube
7. Water level switch
8. Dump valve
9. Dump tank
10. High flow feed pump
11. Low flow feed pump
12. Supporting structure of the scaffold
13. Supporting structure of the core tank
14. Water feed tank for a fine control

Fig. 2-1 Overall structure of the KUCA (C-core)

2.1.2 Core Configurations

The experiments with the D_2O tank were carried out in the core configuration of C35R80D2O(4) as shown in Fig. 2-2(a). A square grid size was 71 mm, and two grid plates were separated by 26.2 mm to see the D_2O tank made of aluminum, 420 mm wide, 820 mm long and 1,120 mm high. The purity of heavy water in the D_2O tank was 99.5%. The total number of fuel plates in the core with the D_2O tank was 384 by loading 40 plates for each fuel frame from 3501 to 3508 and, 16 plates in the frames 3509 through 3512.

Fig. 2-2(b) shows the core configuration of C35G0(4) for the experiments without the D_2O tank where the two grid plates are adjoined without spacers. Forty fuel plates were loaded in each fuel frame 3501 through 3508, and 27 plates in the 3509 through 3512 frames. The total number of fuel plates was 428.

(a) C35R80D2O(4) (b) C35G0(4)

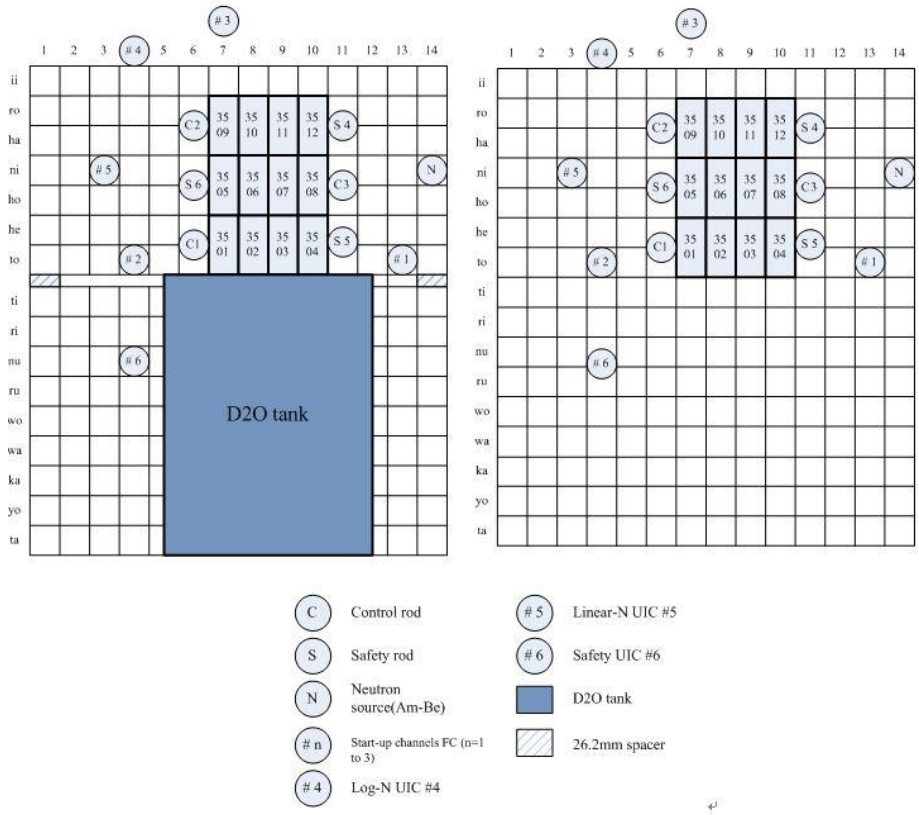

Fig. 2-2 Core configurations of C35R80D2O(4) and C35G0(4)

2.2 The ITRC Estimation

2.2.1 Positive Period Method

One-point kinetic equations with one energy group are as follows:

$$\frac{dn}{dt} = \frac{\rho - \beta_{eff}}{\Lambda} n + \sum_{i}^{6} \lambda_i C_i \tag{2.1}$$

$$\frac{dC_i}{dt} = \frac{\beta_{i,eff}}{\Lambda} n + \lambda_i C_i \quad \text{(i=1...6)} \tag{2.2}$$

where n(t) is number density of neutron, C_i is precursor of delayed neutron of i-th group, λ_i is a decay constant for the delayed neutron , β is a delayed neutron fraction from fission and Λ is neutron generation time. In the critical state, neutron flux can be rewritten when the excess reactivity is inserted, as in the following:

$$\Phi(t) = \sum_{j=1}^{7} A_j e^{\omega t} \tag{2.3}$$

A_j and ω is constant. The substitution of Eq. (2.3) for Eq. (2.1) and Eq. (2.2) results in inhour equation,

$$\rho = \frac{\omega \ell}{1+\omega \ell} + \frac{\omega}{1+\omega \ell} \sum_{i=1}^{6} \frac{\beta_{i,eff}}{\omega + \lambda_i} \tag{2.4}$$

From the inhour equation in Eq. (2.4), the excess reactivity ρ_{ex}, defined by the reactivity adjusted by the partially inserted control rod, corresponding to the measured reactor period t_e at the system temperature can be obtained as follows [10]:

$$\rho_{ex} = \frac{\ell}{t_e + \ell} + \frac{t_e}{t_e + \ell} \sum_{i=1}^{6} \frac{\beta_{i,eff}}{1 + \lambda_i \cdot t_e} \tag{2.5}$$

ℓ is the prompt neutron life time. $\beta_{i,eff}$ and λ_i are the delayed neutron fraction and the decay constant, respectively, of the i-th group delayed neutron precursor. As shown in Table 2-1, the values of ℓ and $\beta_{i,eff}$ are by the McCARD calculations with the continuous-energy cross section libraries from ENDF/B-VII.1, employed by the adjoint-weighted kinetics parameter estimation method [17] for the case 27 in the both configurations. In Table 2-1, RSD denotes the relative standard deviation defined by the standard deviation (SD) divided by the mean and β_{eff} is $\sum_i \beta_{i,eff}$.

To obtain a curve of the excess reactivity for the system temperature *T*, all the results of ρ_{ex} were fitted to a quadratic function for each core configuration [13],

$$\rho_{\text{ex}}(T) \cong aT^2 + bT + c \tag{2.6}$$

where a, b and c are constants. Then the ITRC, value of α_{iso}, can be determined by differentiating Eq. (2.6) as follows:

$$\alpha_{\text{iso}}(T) \cong 2aT + b \tag{2.7}$$

Table 2-1 Kinetics parameters of the two core configurations

Configuration	ℓ (RSD [%])	β_{eff} (RSD [%])	Group Index	$\beta_{i,eff}$ (RSD [%])
C35R80D2O(4)	1.672×10^{-4} (0.004)	7.671×10^{-3} (0.034)	1	2.725×10^{-4} (0.183)
			2	1.393×10^{-3} (0.080)
			3	1.334×10^{-3} (0.086)
			4	2.948×10^{-3} (0.056)
			5	1.216×10^{-3} (0.087)
			6	5.080×10^{-4} (0.136)
C35G0(4)	1.066×10^{-4} (0.002)	7.739×10^{-3} (0.034)	1	2.746×10^{-4} (0.178)
			2	1.405×10^{-3} (0.080)
			3	1.348×10^{-3} (0.080)
			4	2.971×10^{-3} (0.055)
			5	1.228×10^{-3} (0.085)
			6	5.126×10^{-4} (0.136)

2.2.2 Procedures of Experiments

The experiments were carried out in the power-level less than 0.01W so that the fuel and cladding temperatures were considered identical to the light water coolant temperature. The desired temperature of light water was achieved in the dump tank with the use of the heaters or radiator, and the heated or cooled down water was fed into the core tank. The temperatures of light water in the core tank were measured by two thermometers located at 630 mm and 1,438 mm from the bottom of the tank, and those of heavy water were measured from the center and the upper positions of the D_2O tank in the C35R80D2O(4) core. The ITRC experiments were carried out by varying the system temperatures as shown in Table 2-2. From the temperature measurements shown in Table 2-2, differences of the regional temperatures of C35R80D2O(4) and C35G0(4) were found within 0.8˚C and 0.1˚C, respectively.

For each temperature case, the reactivity worth of the inserted control rod was measured by the positive period method through the withdrawal of the rod. Detailed procedures of experiments are as shown in Fig. 2-3:

① The critical state of KUCA-C core is achieved by adjusting the

C3 rod in the condition that the other control rods and all the safety rods were withdrawn to the upper limit position.

② During the power ascension caused by withdrawal of the C3 rod considering operation limit, the doubling time, t_d ($= \ln 2 \cdot t_e$), when the reactor power is doubled, is measured to get the reactor period, t_e, in Eq. (2.5).

③ The critical state of the KUCA C-core is achieved again by inserting the C1 rod.

④ Repeat ① to ③ procedures until the C3 rod is withdrawn to upper limit of the KUCA C-core.

Using Eq. (2.5), Table 2-3 shows the measured excess reactivities, $\rho_{ex}^{exp.}$, in all cases given in Table 2-2 and the constants in Eq. (2.6) estimated by the least-square fitting method for both configurations.

Table 2-2 Measured temperatures (˚C) of the ITRC experiments for the two core configurations

Configuration	Case	CT 5[a)]	CT 6[a)]	DT center[b)]	DT upper[b)]
C35R80D2O(4)	27	26.7	26.7	27.3	27.5
	38	38.1	38.1	38.0	38.0
	40	40.1	40.2	39.9	40.2
	45	44.9	45.0	44.9	45.1
	50	50.4	50.4	50.1	50.3
	55	55.2	55.1	54.6	54.8
	58	58.5	58.4	58.2	58.6
C35G0(4)	19	19.3	19.2		
	27	27.0	27.0		
	30	30.1	30.1		
	40	39.4	39.4		
	45	45.3	45.2		
	50	49.2	49.2		
	55	53.2	53.3		
	60	61.0	61.0		

a) The CT 5 and 6 are the light water temperatures of lower and upper positions, respectively, of the core tank.

b) The DT center and upper are temperatures of the heavy water in the D_2O tank.

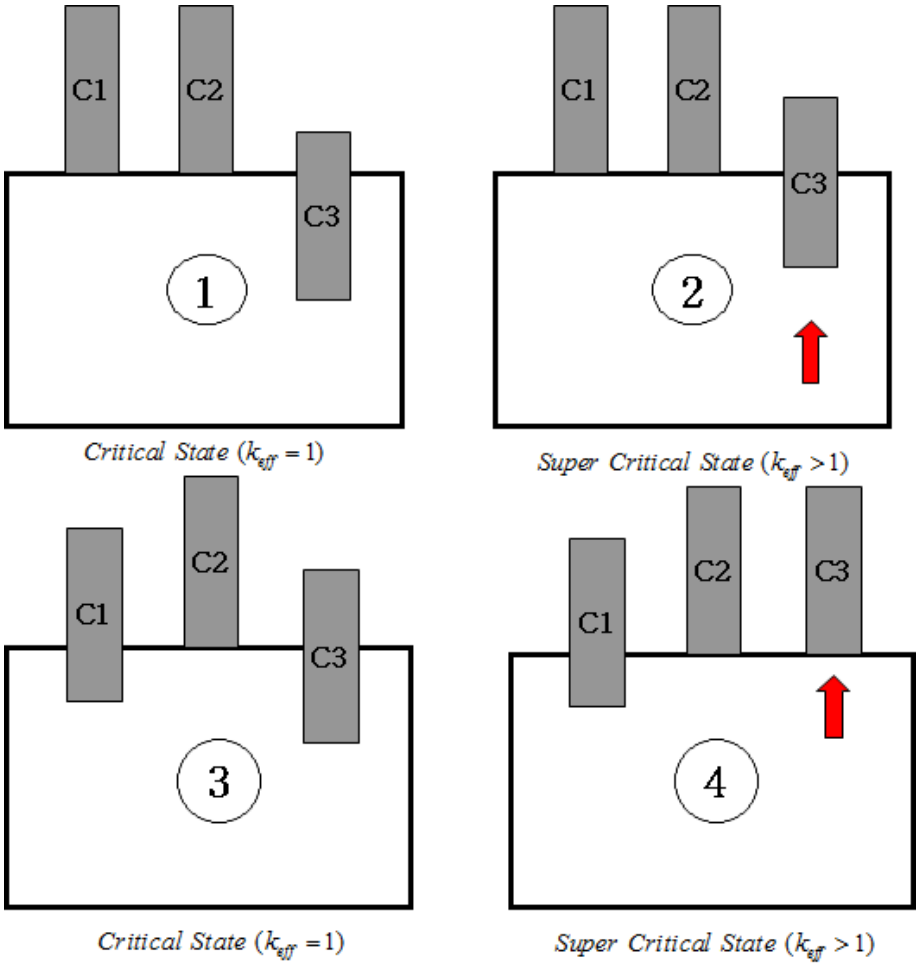

Fig. 2-3 Procedures of experiments

Table 2-3 Measured excess reactivities (pcm) with varying the system temperature for the two core configurations

Configuration	Case	C3 Position [a)]	$\rho_{ex}^{exp.}$	Fitting Constants (SD)
C35R80D2O(4)	27	345.15	289.8	a=-1.733×10^{-1}, (0.012) b= 5.699×10^{0}, (1.000) c= 2.612×10^{2} (20.840)
	38	377.33	223.3	
	40	389.31	213.1	
	45	420.50	167.3	
	50	461.20	114.2	
	55	516.17	52.8	
	58	611.19	6.0	
C35G0(4)	19	317.12	311.6	a=-1.635×10^{-1}, (0.016) b= 6.836×10^{0}, (1.243) c= 2.406×10^{2} (22.861)
	27	320.67	307.6	
	30	328.71	300.5	
	40	358.25	245.7	
	45	383.17	221.5	
	50	406.50	181.4	
	55	438.33	144.8	
	60	508.77	58.1	

a) the withdrawn length (mm) of the control rod from the grid plate.

Chapter 3. MC Adjoint–Weighted Perturbation Method

From the perturbation theory, the first-order change in the fundamental mode eigenvalue k_0, due to the change of the system temperature ΔT (=T-T_0; T: system temperature; T_0: reference temperature), can be expressed as follows [6, 7]:

$$\Delta k \cong < \phi_0^\dagger, \Delta \mathbf{H} S_0 >, \tag{3.1}$$

$$\begin{aligned} \Delta \mathbf{H} S_0 = & \int d\mathbf{P}' H(\mathbf{P}' \to \mathbf{P} \mid T_0 + \Delta T) S_0(\mathbf{P}') \\ & - \int d\mathbf{P}' H(\mathbf{P}' \to \mathbf{P} \mid T_0) S_0(\mathbf{P}') \end{aligned} \tag{3.2}$$

The angular bracket implies the integration over the six-dimensional phase space, (**r**, E, **Ω**) denoted by **P**. $\phi_0^\dagger$ and S_0 denote the fundamental mode adjoint flux and fission source density (FSD), respectively, which are normalized by $\int S_0(\mathbf{P}) d\mathbf{P} = 1$ and $\int \phi_0^\dagger(\mathbf{P}) S_0(\mathbf{P}) d\mathbf{P} = 1$. The kernel $H(\mathbf{P}' \to \mathbf{P} \mid T)$ ($T = T_0$ or $T_0 + \Delta T$) means the number of first-generation fission neutrons born per unit phase space volume about **P**, due to a parent neutron born at $\mathbf{P}'$ for a given temperature T.

In the MC AWP method, $\phi_0^\dagger$ is estimated in the MC forward calculations from its physical meaning ─ the iterated fission probability [18], is expressed by [6]:

$$\phi_0^\dagger(\mathbf{P}) = \lim_{n\to\infty} \frac{1}{{k_0}^n} \int d\mathbf{P}' H^n(\mathbf{P} \to \mathbf{P}') \tag{3.3}$$

Then, the substitution of Eq. (3.3) into Eq. (3.1) and the use of a finite integer n ensuring the convergence of $\phi_0^\dagger$, called the convergence cycle interval of the adjoint flux, Δk can be approximately expressed as follows:

$$\Delta k \cong \frac{1}{{k_0}^n} < \mathbf{H}^n, \Delta\mathbf{H} S_0 > \tag{3.4}$$

In a nuclear reactor core, the system temperature change can be correlated with those in the number densities, the microscopic cross sections, and the transfer probabilities of all the constituent isotopes of the system. Therefore, $\Delta\mathbf{H}S_0$ in Eq. (3.2) can be expressed as follows:

$$\Delta \mathbf{H} S_0 = \int d\mathbf{P}' \left[H \left(\mathbf{P}' \to \mathbf{P} \middle| \begin{array}{l} N^{m,i}(T_0 + \Delta T), \\ \sigma_r^{m,i}(E' \mid T_0 + \Delta T), \\ f_r^{m,i}(E', \mathbf{\Omega}' \to E, \mathbf{\Omega} \mid T_0 + \Delta T) \end{array} \right) \right. \\ \left. - H \left(\mathbf{P}' \to \mathbf{P} \middle| \begin{array}{l} N^{m,i}(T_0), \\ \sigma_r^{m,i}(E' \mid T_0), \\ f_r^{m,i}(E', \mathbf{\Omega}' \to E, \mathbf{\Omega} \mid T_0) \end{array} \right) \right] S_0(\mathbf{P}'), \tag{3.5}$$

$N^{m,i}$, $\sigma_r^{m,i}$ and $f_r^{m,i}$ denote the number density, the effective microscopic cross section and the transfer probability distribution function of *r*-type reaction, respectively, of isotope *i* in region *m*. In this study, the perturbation of k_0 due to the $N^{m,i}$ change is estimated by the first-order DOS method with the adjoint-weighing [6], whereas that from the $\sigma_r^{m,i}$ change is calculated by the AWCS method [7].

3.1 Adjoint-Weighted Differential Operator Sampling (DOS) Method

To derive the adjoint-weighted differential operator sampling method [6], $\mathbf{H}S_0$ in Eq. (3.2) can be expressed explicitly in terms of the transport kernels as follows:

$$\mathbf{H}S_0 = \sum_{j=0}^{\infty} \int dE'' \int d\mathbf{\Omega}'' C_f(\mathbf{r}; E'', \mathbf{\Omega}'' \to E, \mathbf{\Omega}) \\ \times \int d\mathbf{P}_0 K_{s,j}(\mathbf{P}_0 \to \mathbf{r}, E'', \mathbf{\Omega}'') \int d\mathbf{r}' T(E_0, \mathbf{\Omega}_0; \mathbf{r}' \to \mathbf{r}_0) S(\mathbf{r}', E_0, \mathbf{\Omega}_0) \tag{3.6}$$

$K_{s,j}$ is the *j*-th scattering kernel defined by

$$K_{s,0}(\mathbf{P}_0 \to \mathbf{P}) = \delta(\mathbf{P}_0 - \mathbf{P}), \\ K_{s,1}(\mathbf{P}_0 \to \mathbf{P}) = K_s(\mathbf{P}_0 \to \mathbf{P}), \\ K_{s,j}(\mathbf{P}_0 \to \mathbf{P}) = \int d\mathbf{P}_{j-1} \cdots \int d\mathbf{P}_1 K_s(\mathbf{P}_{j-1} \to \mathbf{P}) \cdots K_s(\mathbf{P}_0 \to \mathbf{P}_1); \tag{3.7}$$

where K_s is the transition kernel defined by the product of the scattering kernel, C_s, and the transport kernel, T, are as follows;

$$K_s(\mathbf{P}' \to \mathbf{P}) = T(E, \mathbf{\Omega}; \mathbf{r}' \to \mathbf{r}) \cdot C_s(\mathbf{r}'; E', \mathbf{\Omega}' \to E, \mathbf{\Omega}); \tag{3.8}$$

$$T(E, \mathbf{\Omega}; \mathbf{r}' \to \mathbf{r}) \\ = \frac{\Sigma_t(\mathbf{r}, E)}{|\mathbf{r} - \mathbf{r}'|^2} \exp\left[-\int_0^{|\mathbf{r}-\mathbf{r}'|} \Sigma_t\left(\mathbf{r} - s\frac{\mathbf{r}-\mathbf{r}'}{|\mathbf{r}-\mathbf{r}'|}, E\right) ds \right] \delta\left(\mathbf{\Omega} \cdot \frac{\mathbf{r}-\mathbf{r}'}{|\mathbf{r}-\mathbf{r}'|} - 1 \right) \tag{3.9}$$

$$C_s(\mathbf{r}'; E', \mathbf{\Omega}' \to E, \mathbf{\Omega}) = \sum_{r \neq fis.} \nu_r \frac{\Sigma_r(\mathbf{r}'; E', \mathbf{\Omega}')}{\Sigma_t(\mathbf{r}', E')} f_r(E', \mathbf{\Omega}' \to E, \mathbf{\Omega}) \tag{3.10}$$

ν_r is the average number of neutrons produced from a reaction type *r* and $f_r(E', \mathbf{\Omega}' \to E, \mathbf{\Omega}) dE d\mathbf{\Omega}$ is the probability that a collision of type *r* by a neutron of direction $\mathbf{\Omega}'$ and energy E' will produce a neutron in direction interval $d\mathbf{\Omega}$ about $\mathbf{\Omega}$ with energy in dE about E.

C_f is the fission collision kernel defined by

$$C_f(\mathbf{r};E',\mathbf{\Omega}'\to E,\mathbf{\Omega}) = \frac{\chi(E'\to E)}{4\pi}\cdot\frac{\nu(E')\Sigma_f(\mathbf{r},E')}{\Sigma_t(\mathbf{r},E')} \qquad (3.11)$$

Using Eq. (3.6), $\Delta\mathbf{H}S_0$ in Eq. (3.1) can be expressed as follows:

$$\begin{aligned}
\Delta\mathbf{H}S_0 &= \left(\Delta x\frac{\partial\mathbf{H}}{\partial x}\right)S_0 \\
&= \Delta x\sum_{p=0}^{\infty}\int dE''\int d\mathbf{\Omega}''\int d\mathbf{P}_{p-1}\cdots\int d\mathbf{P}_0\int d\mathbf{r}' \\
&\quad\otimes\frac{\partial}{\partial x}C_f(\mathbf{r};E'',\mathbf{\Omega}''\to E,\mathbf{\Omega})K_s(\mathbf{P}_{p-1}\to\mathbf{r},E'',\mathbf{\Omega}'') \\
&\quad\cdots K_s(\mathbf{P}_0\to\mathbf{P}_1)T(E_0,\mathbf{\Omega}_0;\mathbf{r}'\to\mathbf{r}_0)\}S_0(\mathbf{r}',E_0,\mathbf{\Omega}_0) \\
&= \Delta x\sum_{p=0}^{\infty}\int dE''\int d\mathbf{\Omega}''\int d\mathbf{P}_{p-1}\cdots\int d\mathbf{P}_0\int d\mathbf{r}'\ u^p(\mathbf{r}',E_0,\mathbf{\Omega}_0\to\mathbf{P}) \\
&\quad\otimes\{C_f(\mathbf{r};E'',\mathbf{\Omega}''\to E,\mathbf{\Omega})K_s(\mathbf{P}_{p-1}\to\mathbf{r},E'',\mathbf{\Omega}'') \\
&\quad\cdots K_s(\mathbf{P}_0\to\mathbf{P}_1)T(E_0,\mathbf{\Omega}_0;\mathbf{r}'\to\mathbf{r}_0)\}S_0(\mathbf{r}',E_0,\mathbf{\Omega}_0);
\end{aligned} \qquad (3.12)$$

$$\begin{aligned}
u^p(\mathbf{r}',E_0,\mathbf{\Omega}_0\to\mathbf{P}) = u_f(\mathbf{r};E'',\mathbf{\Omega}''\to E,\mathbf{\Omega}) + u_K(\mathbf{P}_{p-1}\to\mathbf{r},E'',\mathbf{\Omega}'') \\
+\sum_{k=0}^{p-2}u_K(\mathbf{P}_k\to\mathbf{P}_{k+1}) + u_T(E_0,\mathbf{\Omega}_0;\mathbf{r}'\to\mathbf{r}_0),
\end{aligned} \qquad (3.13)$$

$$u_f(\mathbf{r};E'',\mathbf{\Omega}''\to E,\mathbf{\Omega}) = \frac{1}{C_f(\mathbf{r};E'',\mathbf{\Omega}''\to E,\mathbf{\Omega})}\frac{\partial C_f(\mathbf{r};E'',\mathbf{\Omega}''\to E,\mathbf{\Omega})}{\partial x} \qquad (3.14)$$

$$u_K(\mathbf{P}_k\to\mathbf{P}_{k+1}) = \frac{1}{K_s(\mathbf{P}_k\to\mathbf{P}_{k+1})}\frac{\partial K_s(\mathbf{P}_k\to\mathbf{P}_{k+1})}{\partial x}, \qquad (3.15)$$

$$u_T(E_0, \mathbf{\Omega}_0; \mathbf{r}' \to \mathbf{r}_0) = \frac{1}{T(E_0, \mathbf{\Omega}_0; \mathbf{r}' \to \mathbf{r}_0)} \frac{\partial T(E_0, \mathbf{\Omega}_0; \mathbf{r}' \to \mathbf{r}_0)}{\partial x} .$$

(3.16)

$\Delta \mathbf{H} S_0$ in Eq. (3.12) can be scored in the MC random walk process. In this study, $\Delta \mathbf{H} S_0$ of DOS method indicates the change in the number of neutrons born per unit phase space volume about **P** in cycle as a result of perturbation in the density x by Δx caused by temperature change.

3.2 Adjoint-Weighted Correlated Sampling Method

The first term of right hand side of Eq. (3.2) can be rewritten using Eq. (3.6) as

$$\mathbf{H}^* S_0 \equiv \int d\mathbf{P}' H(\mathbf{P}' \to \mathbf{P} \mid T_0 + \Delta T) S_0(\mathbf{P}') \tag{3.17}$$

$$\begin{aligned} \mathbf{H}^* S_0 = & \sum_{j=0}^{\infty} \int dE'' \int d\mathbf{\Omega}'' C_f^*(\mathbf{r}; E'', \mathbf{\Omega}'' \to E, \mathbf{\Omega}) \\ & \times \int d\mathbf{P}_0 K_{s,j}^*(\mathbf{P}_0 \to \mathbf{r}, E'', \mathbf{\Omega}'') \int d\mathbf{r}' T^*(E_0, \mathbf{\Omega}_0; \mathbf{r}' \to \mathbf{r}_0) S(\mathbf{r}', E_0, \mathbf{\Omega}_0) \end{aligned} \tag{3.18}$$

The asterisked kernels in Eq. (3.17) refer to $\mathbf{H} S_0$ in the perturbed system. The rest of notation follows standard. By subtraction of Eq. (3.6) from Eq. (3.18), $\Delta \mathbf{H} S_0$ can be expressed by [3,4]

$$\begin{aligned}\Delta\mathbf{H}S_0 = \sum_{j=0}^{\infty}\int dE''\int d\mathbf{\Omega}''\int d\mathbf{P}_0\; u^j(\mathbf{P}'\to\mathbf{P}) \\ \times C_f(\mathbf{r};E'',\mathbf{\Omega}''\to E,\mathbf{\Omega})K_{s,j}(\mathbf{P}_0\to\mathbf{r},E'',\mathbf{\Omega}'') \\ \times\int d\mathbf{r}'T(E_0,\mathbf{\Omega}_0;\mathbf{r}'\to\mathbf{r}_0)S(\mathbf{r}',E_0,\mathbf{\Omega}_0)\end{aligned} \tag{3.19}$$

$$\begin{aligned}u^j(\mathbf{P}'\to\mathbf{P}) = \frac{C_f^*(\mathbf{r};E'',\mathbf{\Omega}''\to E,\mathbf{\Omega})}{C_f(\mathbf{r};E'',\mathbf{\Omega}''\to E,\mathbf{\Omega})} \\ \times\prod_{p=0}^{j-1}\frac{K_s^*(\mathbf{P}_p\to\mathbf{P}_{p+1})}{K_s(\mathbf{P}_p\to\mathbf{P}_{p+1})}\cdot\frac{T^*(E_0,\mathbf{\Omega}_0;\mathbf{r}'\to\mathbf{r}_0)}{T(E_0,\mathbf{\Omega}_0;\mathbf{r}'\to\mathbf{r}_0)}-1\end{aligned} \tag{3.20}$$

Eq. (3.19) indicate that $\Delta\mathbf{H}S_0$ of CS method can be calculated by cumulating u^j for all the neutron tracks.

3.2.1 Free Gas Thermal Treatment

The transfer probability, $f_r^{m,i}(E',\mathbf{\Omega}'\to E,\mathbf{\Omega}\,|\,T)$, in the transport kernel, C_s, in Eq. (3.10) is usually treated to be constant, since the Doppler-broadening of transfer probability is negligible in fast neutron range. However, scattering spectrum of thermal neutrons is greatly influenced by the Doppler-broadening of transfer probability. To take into account of the Doppler-broadened transfer probability, $f_r^{m,i}(E',\mathbf{\Omega}'\to E,\mathbf{\Omega}\,|\,T)$ in the thermal neutron range, the free gas model with constant cross section [8] is applied, unless a proper TSL of isotope

i is given. Therefore, perturbation of k_0 from the $f_r^{m,i}$, change of nuclides except hydrogen and deuterium, of which TSLs are used, are estimated by the AWCS for the constant cross section model [7].

3.2.2 Stochastic Mixing Method

For the Doppler-broadening of thermal scattering cross sections of hydrogen and deuterium in coolant at T, the stochastic mixing method [16] is applied. It takes a cross section library at T_1 ($<T$) by proportion of p ($=(T_2-T)/(T_2-T_1)$) and a library at T_2 ($>T$) with proportion (1-p). When the system temperature is varied from T to $T+\Delta T$, probability to select the T_1 library is changed into p^* ($= p-\Delta T/(T_2-T_1)$) and as a result, the probability for the T_2 library is changed into (1- p^*) from (1-p). In the CS method with the adjoint-weighting, in order to estimate the k_0 change from the p change, $\Delta\mathbf{H}S_0$ is calculated from the adjustment factor [3] at each track, defined by the ratio of perturbed transport kernel to unperturbed one. Then the adjustment factor at i-th track, a_i, in the stochastic mixing is simply expressed with the use of ratio of the library selection probability as follows:

$$a_i = \begin{cases} p^* / p & \text{when library } T_1 \text{ is selected,} \\ (1-p^*)/(1-p) & \text{when library } T_2 \text{ is selected.} \end{cases} \tag{3.21}$$

Chapter 4. Numerical Results

4.1 Comparison of Excess Reactivity

Before the ITRC analyses by the MC perturbation methods, the measured excess reactivities are compared with the calculated ones by subtracting two reactivity values estimated by the McCARD eigenvalue calculations at both the critical position and the upper limit of the C3 rod at the temperature cases shown in Table 2-2 and Table 2-3. McCARD calculations are performed on 2,000 active cycles with 1,000,000 histories per cycle. In this study, all the McCARD calculations are conducted with the continuous-energy cross section libraries produced by NJOY [19] from ENDF/B-VII.1, whereas TSLs of hydrogen and deuterium in coolant are produced from ENDF/B-VII.0. Table 4-1 shows the comparison of the excess reactivities at the different temperature cases obtained from the measurements and the McCARD direct subtractions. From the results in Table 4-1, absolute maximum values of the differences between the excess reactivity calculated by McCARD ρ_{ex}^{MC}, and the measurement $\rho_{ex}^{exp.}$ are 21.3 and 19.8 pcm at 27˚C of C35R80D2O(4) and C35G0(4) cores, respectively. These values are

corresponding to the relative differences of 7.3% and 6.4% between the measurements and the calculations. From the ρ_{ex}^{MC} data in Table 4-1, the quadratic curves of Eq. (2.6) are fitted as follows:

$$\rho_{ex}^{MC}(T) \cong \begin{cases} -18.09(0.010)T^2 + 6.829(0.899)T + 215.6(18.735) & \text{for C35R80D2O,} \\ -18.04(0.007)T^2 + 7.713(0.524)T + 240.6(9.636) & \text{for C35G0.} \end{cases}$$

(4.1)

Table 4-1 Comparison of the excess reactivities (pcm) for the two core configurations

Configuration	Case	$\rho_{ex}^{exp.}$	ρ_{ex}^{MC} (SD)	$\rho_{ex}^{MC} - \rho_{ex}^{meas.}$
C35R80D2O(4)	27	289.8	268.5 (2.8)	-21.3
	38	223.3	214.6 (2.8)	-8.7
	40	213.1	200.9 (2.8)	-12.2
	45	167.3	152.8 (2.8)	-14.5
	50	114.2	107.5 (2.8)	-6.7
	55	52.8	48.4 (2.8)	-4.4
	58	6.0	1.0 (2.8)	-5.0
C35G0(4)	19	311.6	323.4 (2.8)	11.8
	27	307.6	327.4 (2.8)	19.8
	30	300.5	308.7 (2.8)	8.2
	40	245.7	264.9 (2.8)	19.2
	45	221.5	224.9 (2.8)	3.4
	50	181.4	188.7 (2.8)	7.3
	55	144.8	138.7 (2.8)	-6.1
	60	58.1	57.1 (2.8)	-1.0

Fig. 4-1 shows the comparisons between $\rho_{ex}^{exp.}(T)$ and $\rho_{ex}^{MC}(T)$ on the fitted quadratic curves. In Fig. 4-1, the solid and dashed lines represent the results of the measurements and the McCARD calculations, respectively. From the results in Fig. 4-1, we can see that the quadratic polynomial fits fairly well in the excess reactivity according to the system temperature.

Fig. 4-2 reveals the comparisons between the temperature-dependent ITRC $\alpha_{iso}(T)$, with the fitting constants in Table 2-3 from measurements $\alpha_{iso}^{exp.}(T)$, and with those in Eq. (4.1) from the McCARD calculations $\alpha_{iso}^{MC,fit}(T)$, which are calculated by Eq. (2.7). In Fig. 4-2, the error bar indicates the 90% confidence interval estimated by the uncertainties of the fitting constants. From the results in Fig. 4-2, the McCARD excess reactivity calculations demonstrated a remarkable reconstruction of the experimental results of the temperature-dependent ITRC with the 90% confidence interval.

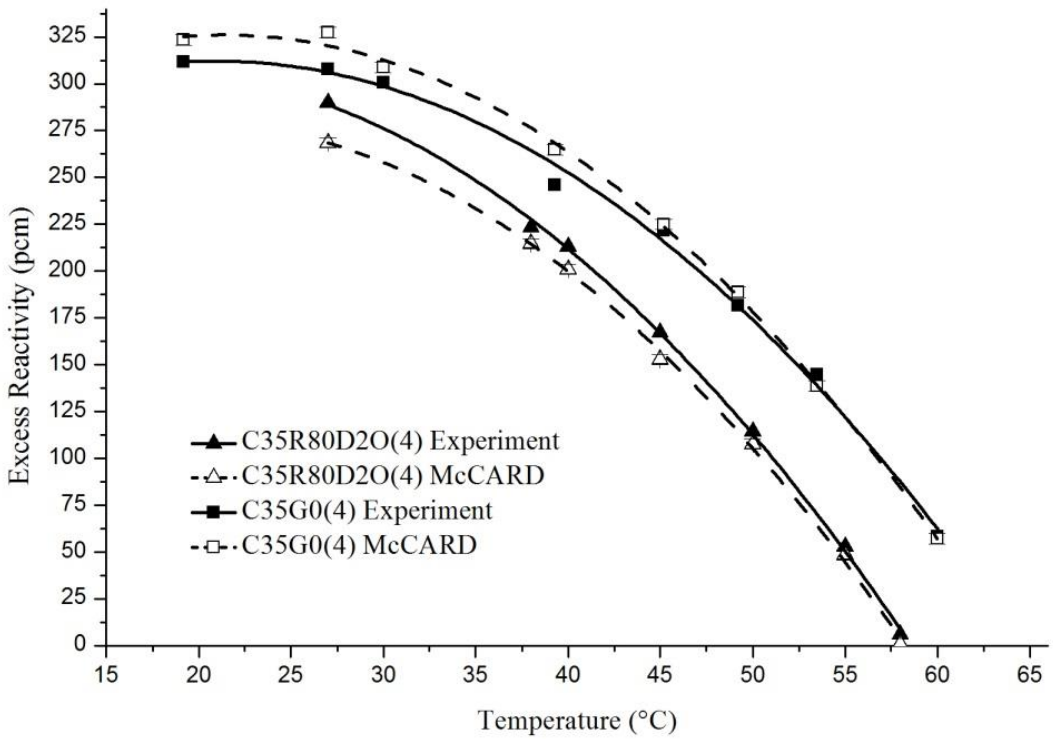

Fig. 4-1 Comparisons of excess reactivities varying the system temperature for C35R80D2O(4) and C35G0(4) cores

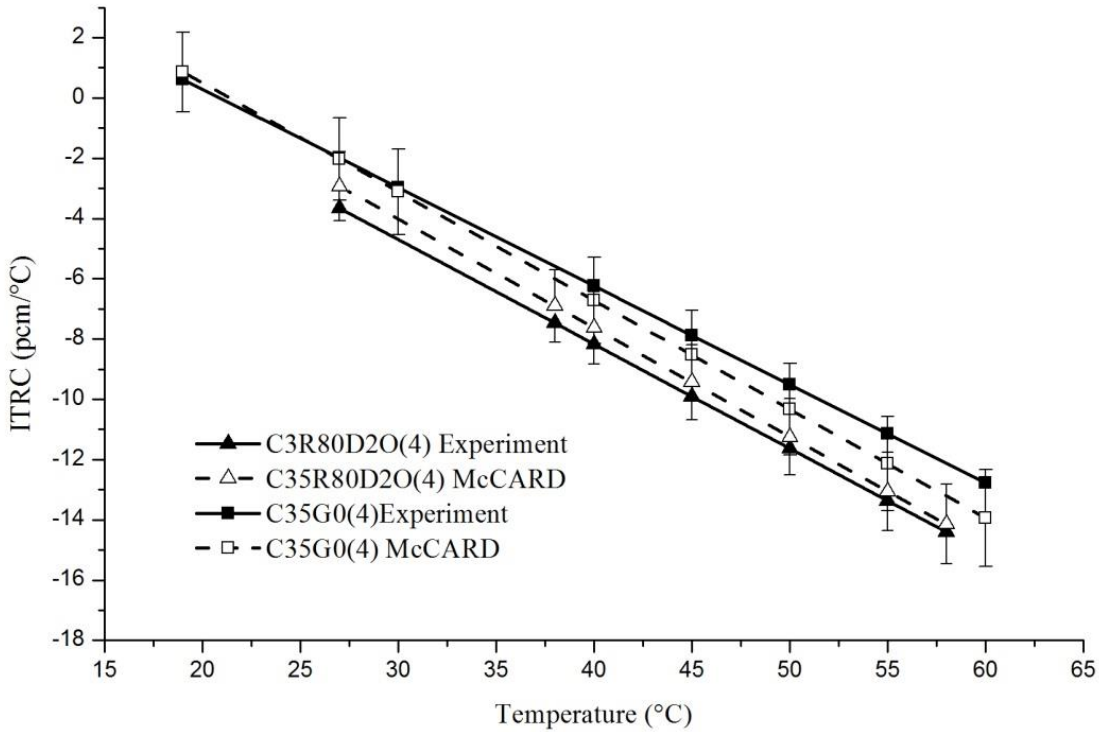

Fig. 4-2 Comparisons between the temperature-dependent ITRC estimated by experiments and the MC direct subtractions

4.2 MC Perturbation Analyses

For the ITRC estimation, the McCARD perturbation calculations for isotopic changes in the density and the microscopic cross sections are conducted for four regions of the C35R80D2O(4) core: fuel, moderator, reflector and D_2O regions. With the C35G0(4) core where a D_2O tank is not installed, only the fuel, moderator and reflector are considered. The moderator region is defined as the coolant between the fuel plates, while the reflector regions as H_2O surrounding the fuel frames axially and radially. In the perturbation calculations, the effects of density change are considered only for the moderator, reflector and D_2O regions. The McCARD AWP calculations are performed on 2,000 active cycles in number density perturbation runs and 20,000 active cycles in the microscopic cross section ones with the same 100,000 histories per cycle at five temperature points (27, 40, 45, 50 and 55˚C) for a temperature variation of 1˚C. For the comparison, the reference ITRCs by the direct subtraction method for the 5˚C temperature difference are obtained beforehand with 1,000,000 histories per cycle in 2,000 active cycles at the five temperature points.

Table 4-2 and Table 4-3 show the contributions of the density

and cross section changes of constituent isotopes in the divided regions to the ITRC calculated by the MC AWP method at 27˚C and 50˚C for C35R80D2O(4) and C35G0(4), respectively. In Table 4-2 and Table 4-3, the ITRC is obtained by summing up all the region-wise isotopic contributions to the ITRC. $^{1}H_{TSL}$ and $^{2}H_{TSL}$ indicate the contributions of thermal scattering cross section changes of hydrogen and deuterium, respectively. From the results in Table 4-2 and Table 4-3, two perturbation of the density and the thermal scattering cross sections of hydrogen are clearly observed in the main contributor of the ITRCs in both core configurations.

Table 4-2 Sensitivities of the ITRC at 27.5˚C and 50.5˚C for the C35R80D2O(4) core

Region	Isotope	Contribution of each isotope to the ITRC (pcm/˚C)			
		Density AWP (RSD [%])		Cross section AWP (RSD [%])	
		27.5˚C	50.5˚C	27.5˚C	50.5˚C
Fuel	^{234}U			-0.002 (3.1)	-0.002 (3.1)
	^{235}U			-0.043 (0.1)	-0.042 (0.1)
	^{236}U			0.000 (28.7)	0.000 (30.1)
	^{238}U			-0.023 (1.0)	-0.020 (1.0)
	^{27}Al			0.000 (29.6)	0.000 (122.1)
	Total			-0.068 (0.6)	-0.065 (0.6)
Moderator	^{1}H	-8.617 (0.3)	-13.946 (0.3)	0.016 (0.1)	0.016 (0.1)
	$^{1}H_{TSL}$			-4.085 (48.0)	-6.480 (18.8)
	^{16}O	-1.465 (0.5)	-2.368 (0.5)	-0.008 (4.7)	-0.005 (7.1)
	Total	-10.083 (0.2)	-17.033 (0.3)	-4.077 (48.1)	-6.468 (18.8)
Reflector	^{1}H	0.288 (3.7)	0.431 (4.3)	0.000 (2.0)	0.000 (1.3)
	$^{1}H_{TSL}$			12.174 (4.9)	10.474 (3.4)
	^{16}O	-0.656 (0.4)	-1.074 (0.4)	-0.006 (3.7)	-0.006 (4.0)
	Total	-0.368 (3.0)	-0.642 (3.0)	12.168 (4.9)	10.469 (3.4)
D_2O tank	^{1}H	0.001 (86.8)	0.005 (39.2)	0.000 (0.4)	0.000 (0.4)
	$^{1}H_{TSL}$			-0.204 (158.0)	-0.130 (147.0)
	^{2}H	-0.526 (0.8)	-1.205 (0.8)	0.000 (0.8)	0.000 (0.8)
	$^{2}H_{TSL}$			0.466 (68.6)	0.489 (39.2)
	^{16}O	-0.300 (1.0)	-0.694 (1.0)	0.012 (3.6)	0.011 (6.4)
	Total	-0.825 (0.5)	-1.884 (1.1)	0.273 (165.5)	0.368 (73.5)

Table 4-3 Sensitivities of the ITRC at 27.5˚C and 50.5˚C for the C35G0(4) core

Region	Isotope	Contribution of each isotope to the ITRC (pcm/˚C)			
		Density AWP (RSD[%])		Cross section AWP (RSD[%])	
		27.5˚C	50.5˚C	27.5˚C	50.5˚C
Fuel	^{234}U			-0.002 (3.1)	-0.002 (3.0)
	^{235}U			-0.043 (1.1)	-0.045 (0.9)
	^{236}U			0.000 (21.2)	0.000 (34.7)
	^{238}U			-0.021 (1.0)	-0.022 (1.0)
	^{27}Al			0.000 (47.5)	0.000 (19.3)
	Total			-0.065 (0.7)	-0.068 (0.7)
Moderator	^{1}H	-8.910 (0.2)	-14.573 (0.2)	0.016 (0.1)	0.017 (0.2)
	$^{1}H_{TSL}$			-4.071 (48.0)	-5.684 (21.2)
	^{16}O	-1.499 (0.3)	-2.460 (0.5)	-0.008 (4.7)	-0.006 (6.5)
	Total	-10.409 (0.1)	-17.033 (0.2)	-4.062 (48.1)	-5.673 (21.3)
Reflector	^{1}H	0.263 (3.3)	0.439 (4.8)	0.000 (1.6)	0.000 (1.2)
	$^{1}H_{TSL}$			15.182 (4.3)	12.937 (3.1)
	^{16}O	-0.907 (0.3)	-1.510 (0.3)	-0.009 (3.0)	-0.006 (4.2)
	Total	-0.644 (1.4)	-1.071 (2.0)	15.174 (4.3)	12.932 (3.1)

Table 4-4 shows the comparisons of the values of ITRC by the experiments $\alpha_{iso}^{exp.}$, the McCARD direct subtractions $\alpha_{iso}^{MC,fit}$, and the McCARD perturbation calculations $\alpha_{iso}^{MC,pert.}$ at five temperature points. From Table 4-4, the MC AWP methods reproduce well the measured ITRC results within its 90% confidence interval. Fig. 4-3 and Fig. 4-4 show $\alpha_{iso}^{MC,pert.}$, $\alpha_{iso}^{MC,sub.}$ and the contributions of the density and cross section perturbations to $\alpha_{iso}^{MC,pert.}$ for C35R80D2O(4) and C35G0(4), respectively. From the results in Fig. 4-3 and Fig. 4-4, the MC AWP methods show good agreement with the MC direct subtraction within similar uncertainty. And the mean estimates of the ITRC in the both cores are negative with negative gradients in the temperatures less than 27˚C, and they can be successfully obtained by competitions between the positive effect of the microscopic cross section changes and the negative one due to the density changes from the AWP methods.

Table 4-4 Comparison of the ITRCs (pcm/˚C) for C35R80D2O(4) and C35G0(4)

Configuration	Case	$\alpha_{iso}^{exp.}$	$\alpha_{iso}^{MC,fit}$ (SD)	$\alpha_{iso}^{MC,pert.}$ (SD)
C35R80D2O(4)	27.5	-3.8	-5.2 (0.7)	-2.6 (2.1)
	40.5	-8.3	-9.5 (0.7)	-7.8 (1.3)
	45.5	-10.1	-11.2 (0.8)	-11.2 (1.3)
	50.5	-11.8	-12.9 (0.8)	-12.5 (1.3)
	55.5	-13.5	-14.5 (0.8)	-16.2 (1.3)
C35G0(4)	27.5	-2.2	-2.0 (0.8)	-1.1 (2.0)
	40.5	-6.4	-6.7 (0.9)	-5.9 (1.3)
	45.5	-8.0	-8.5 (0.9)	-7.5 (1.2)
	50.5	-9.7	-10.3 (0.9)	-11.5 (1.2)
	55.5	-11.3	-12.1 (0.9)	-11.6 (1.3)

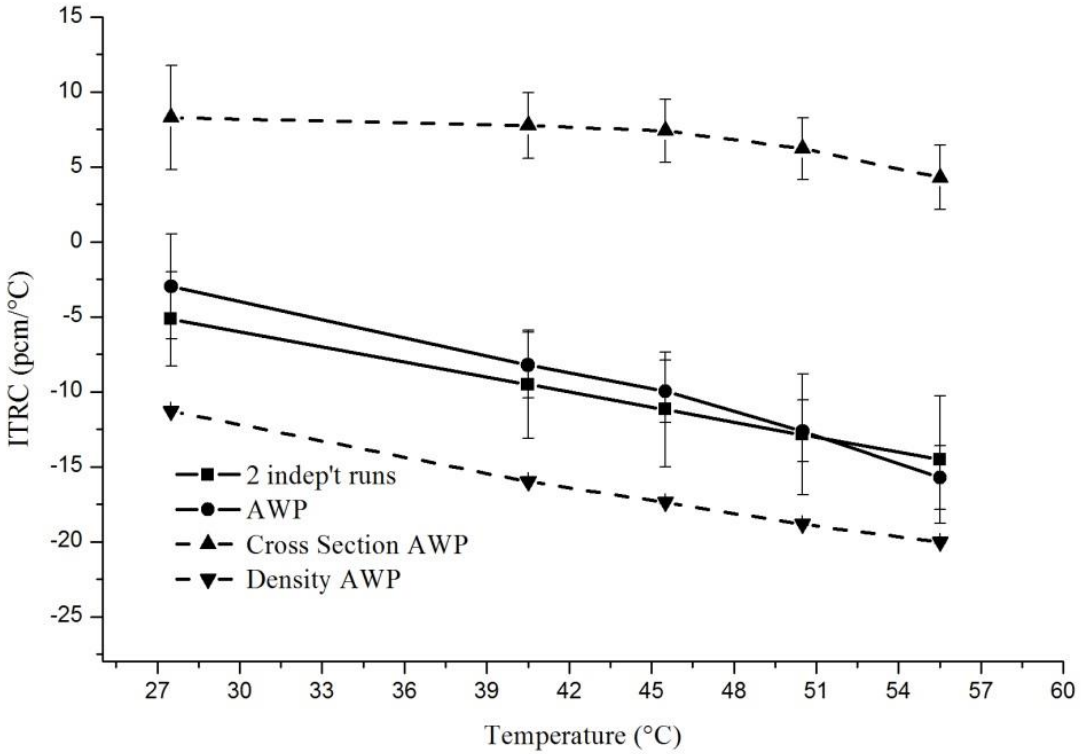

Fig. 4-3 The ITRC contributions of the density and cross section perturbations in C35R80D2O(4) core

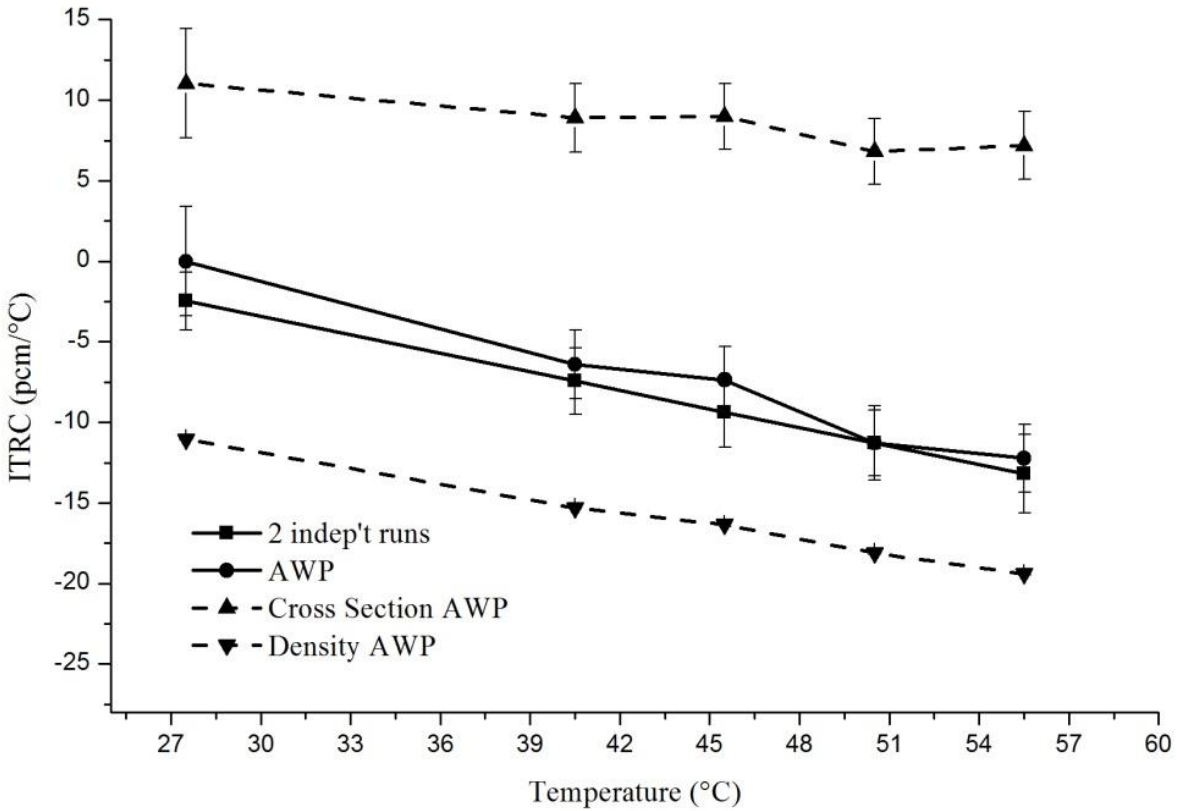

Fig. 4-4 The ITRC contributions of the density and cross section perturbations in C35G0(4) core

Fig. 4-5 and Fig. 4-6 show the region-wise and isotope-wise effects of the density perturbation caused by the temperature change for C35R80D2O(4) and C35G0(4), respectively. From the results in Fig. 4-5 and Fig. 4-6, the main contributors of the negative ITRC and its negative gradient in both cores are considered dominant over the degradation of the neutron moderation caused by the decrease in the hydrogen density of the moderator region. Also, the oxygen in the moderator region is also a significant contributor of the negative ITRC, whereas the effects of the density perturbation in the reflector and D_2O regions on the ITRC are relatively small. These facts demonstrate that a positive effect caused by the density decrease of hydrogen in the reflector region since the absorption reactions by hydrogen was reduced in the reflector.

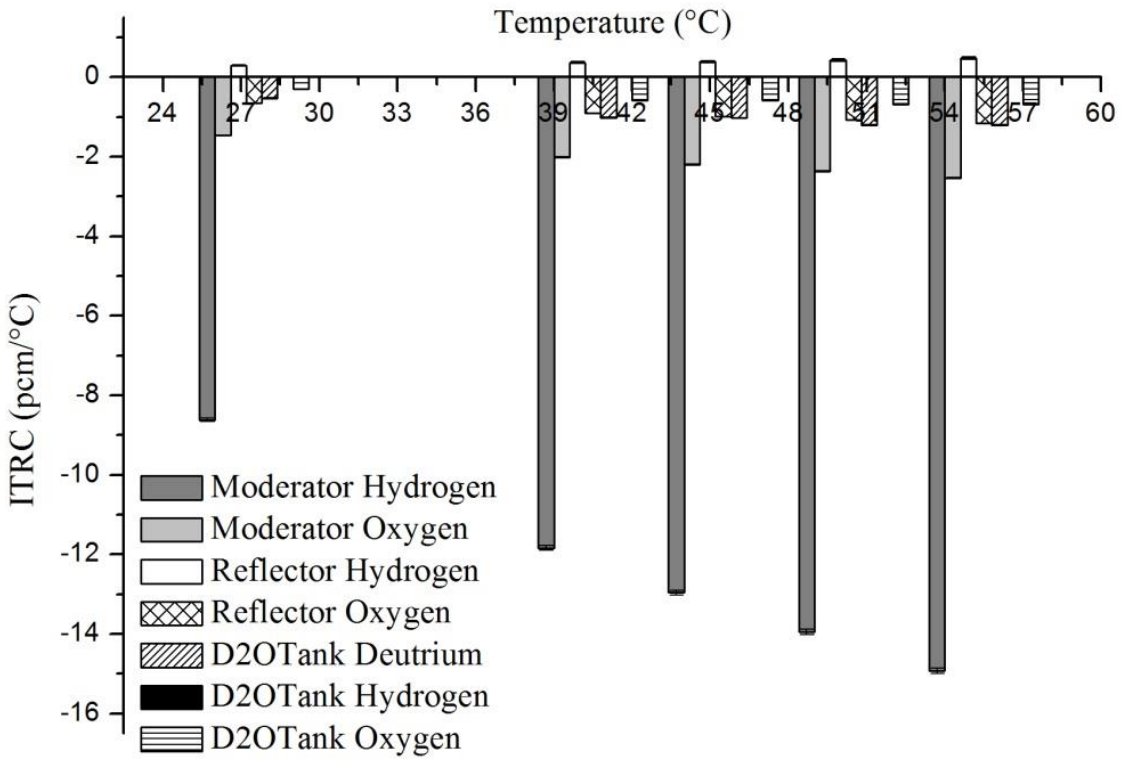

Fig. 4-5 Region-dependent contributions of the isotopic density perturbations to the ITRC for C35R80D2O(4)

core

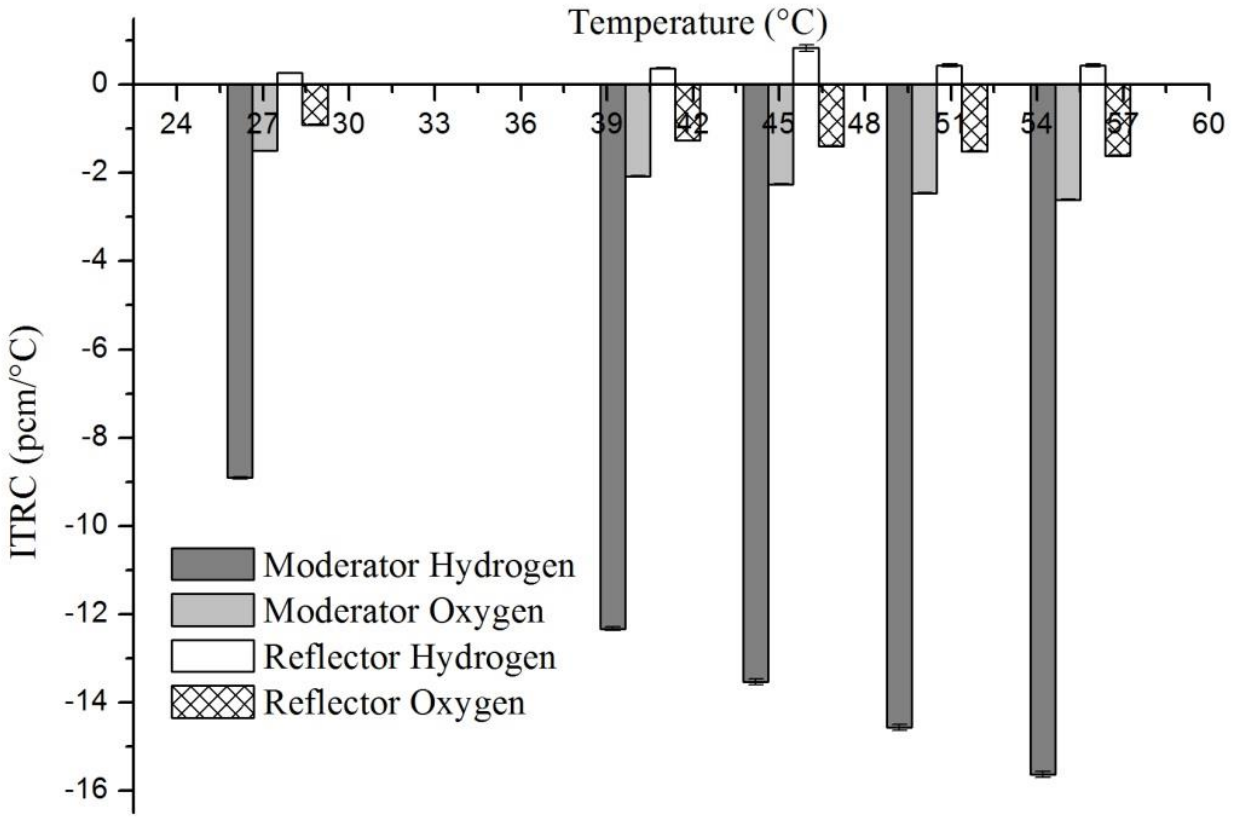

Fig. 4-6 Region-dependent contributions of the isotopic density perturbations to the ITRC for C35G0(4) core

Fig. 4-7 and Fig. 4-8 show the region-wise effects of the microscopic cross section perturbations caused by the temperature change for C35R80D2O(4) and C35G0(4), respectively. And for an investigation of the region-wise and isotope-wise effects on the ITRC with reliable uncertainty, the McCARD AWCS calculations in Fig. 4-7 and Fig. 4-8 are performed on 50,000 total active cycles in the microscopic cross section perturbations with 100,000 histories per cycle at five temperature points. From the Fig. 4-7 and Fig. 4-8, the perturbation of the thermal scattering cross sections of hydrogen in the moderator and reflector regions is dominant over the cross section change in the hydrogen, whereas the Doppler broadening effect of the uranium fuel is negligible in the ITRC. Fig. 4-9 and Fig. 4-10 show the estimated thermal neutron flux spectrum in each region with different temperatures at 27˚C and 60˚C, respectively at both cores. Note that spectrums of thermal neutron fluxes are normalized to unity at the core region at 27˚C. From the results, the large contribution of the thermal scattering cross section change of hydrogen is caused by the spectrum hardening of the thermal neutron due to the increase of its up-scattering probability. These up-scattered thermal neutrons cause in the reflector region decrease of absorption of hydrogen while that in the moderator

region decreases the fission reaction in fuel. This thermal neutron spectral shift effect is attributed to the positive ITRC in the reflector region [1].

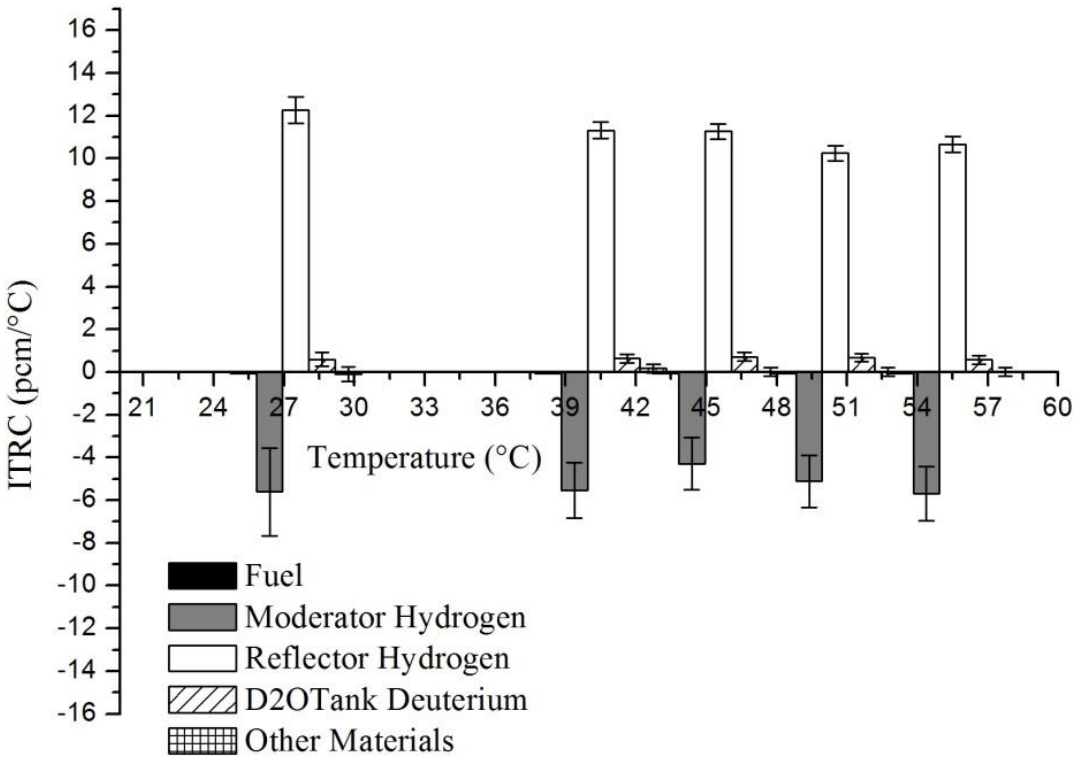

Fig. 4-7 Region-dependent contributions of the microscopic cross section perturbations to the ITRC for

C35R80D2O(4) core

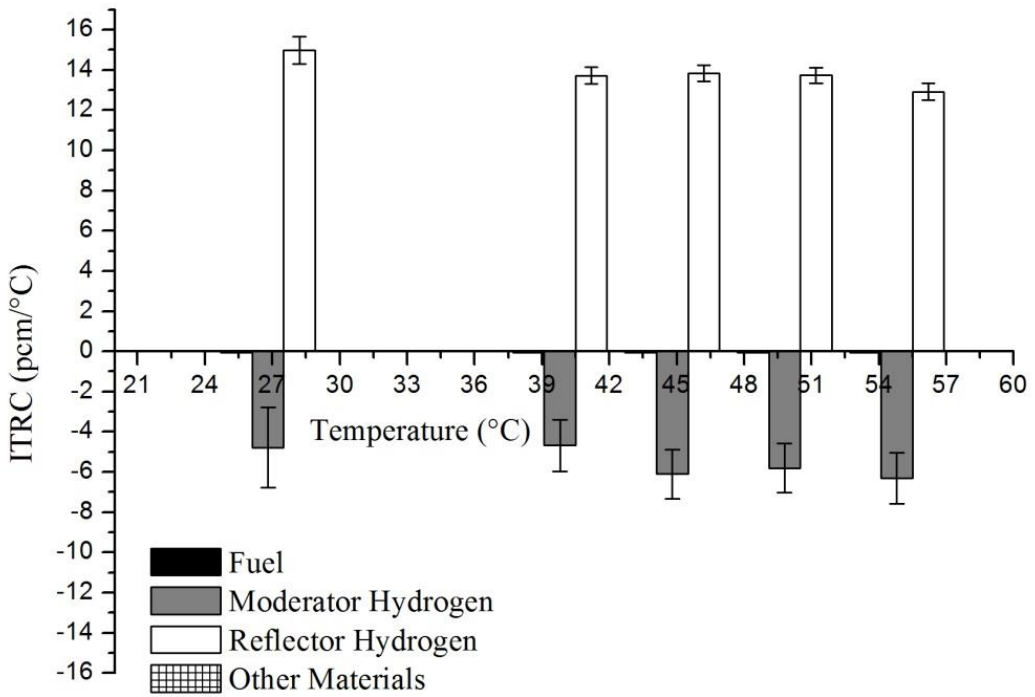

Fig. 4-8 Region-dependent contributions of the microscopic cross section perturbations to the ITRC for

C35G0(4) core

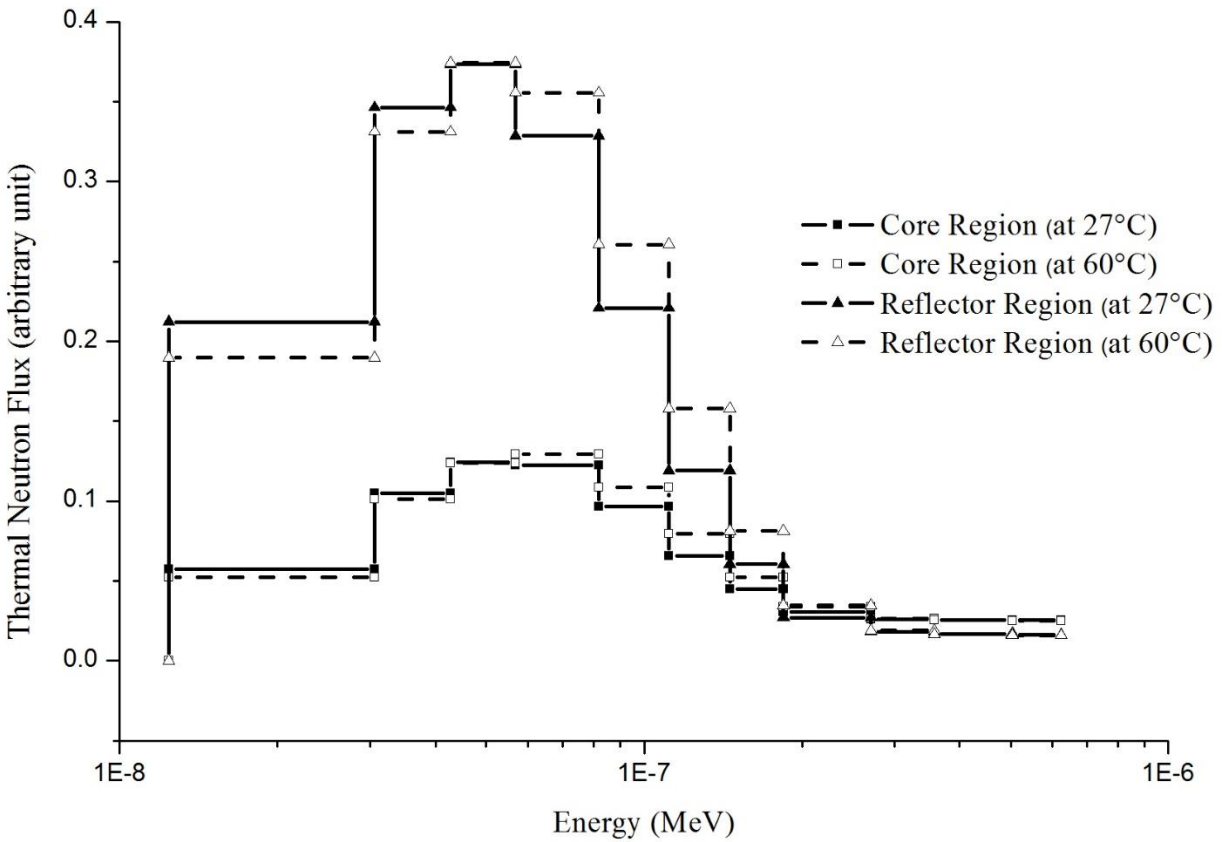

Fig. 4-9 Calculated thermal neutron flux spectrums (<0.625eV) of C35R80D2O(4) core

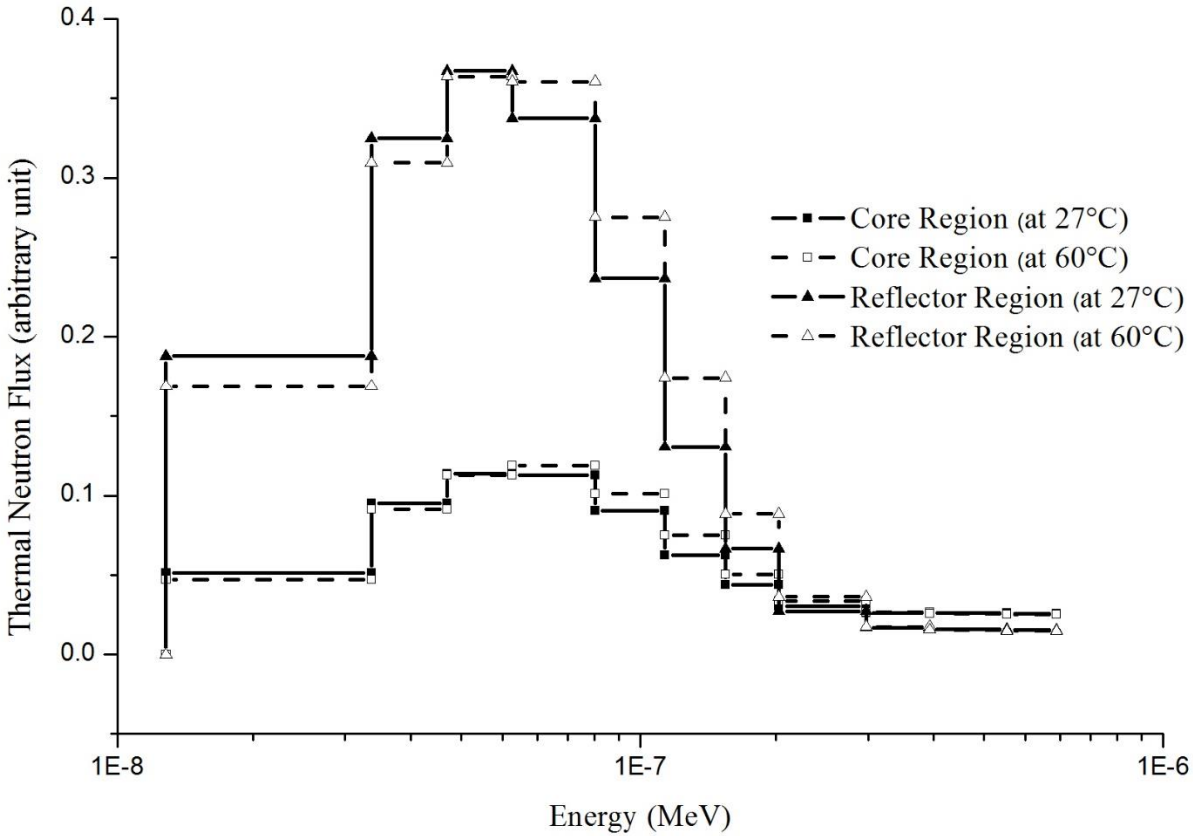

Fig. 4-10 Calculated thermal neutron flux spectrums (<0.625eV) of C35G0(4) core

Chapter 5. Conclusions

The ITRCs, measured at the KUCA C-cores, C35R80D2O(4) and C35G0(4) ─with and without the D_2O tank─ are estimated by the McCARD eigenvalue calculations. From the comparison between the measured and calculated excess reactivity, it is demonstrated that the McCARD direct subtraction method produces accurate excess reactivity within the maximum difference of 21.3 pcm at 27˚C. Then, the region-wise and isotope-wise contributions of the density and cross section perturbations due to the temperature changes, are investigated by the MC AWP calculations. From these detailed sensitivities to the C-core ITRC, first, the ITRC in each core consists of negative effects due to the density changes and positive ones owing to the microscopic cross section changes. Second, the negative ITRC and its negative gradient are dominant over the decrease in the hydrogen number density at the moderator region as the system temperature increased. Third, the positive contribution to the ITRC is attributed to the thermal spectrum hardening due to the increase of up-scattering probability of hydrogen at the reflector region. This indicates that a transfer probability change of hydrogen in thermal scattering cross section governs the ITRC at the

reflector region. The AWCS with stochastic mixing method clearly shows the effect of thermal scattering section change at the KUCA C-core.

References

1. S. Shiroya, M. Mori, and K. Kanda, “Analysis of Experiment on Temperature Coefficient of Reactivity in Light-Water-Moderated and Heavy-Water-Reflected Cylindrical Core Loaded with Highly-Enriched-Uranium or Medium-Enriched-Uranium Fuel,” *J. Nucl. Sci. Technol.*, **33**[3], 211 (1996).

2. L. B. Miller, “Monte Carlo Analysis of Reactivity Coefficients in Fast Reactors; General Theory and Applications,” ANL-7307 (TID-4500), Argonne National Laboratory, IL (1967).

3. H. Rief, “Generalized Monte Carlo Perturbation Algorithms for Correlated Sampling and a Second-Order Taylor Series Approach,” *Ann. Nucl. Energy*, **11**, 455 (1984).

4. Y. Nagaya, T. Mori, “Impact of Perturbed Fission Source on the Effective Multiplication Factor in Monte Carlo Perturbation Calculations,” *J. Nucl. Sci. Technol.*, **42**[5], 428 (2005).

5. B. Kiedrowski, F. B. Brown, P. P. H. Wilson, “Adjoint-Weighted Tallies for k-Eigenvalue Calculations with Continuous-Energy

Monte Carlo," *Nucl. Sci. Eng.*, **168**, 226 (2011).

6. H. J. Shim, C. H. Kim, "Adjoint Sensitivity and Uncertainty Analyses in Monte Carlo Forward Calculations," *J. Nucl. Sci. Technol.*, **48**[12], 1453 (2011).

7. H. J. Shim, C. H. Kim, "Monte Carlo Fuel Temperature Coefficient Estimation by an Adjoint-Weighted Correlated Sampling Method," *Nucl. Sci. Eng.*, 177 ,184 (2014).

8. J. F. Briesmeister, "MCNP-a general Monte Carlo N-particle transport code, version 4B," LA-13181, *Los Alamos National Laboratory* (1997).

9. B. Becker, R. Dagan, C. H. M. Broeders, "Proof and Implementation of the Stochastic Formula for Ideal Gas, Energy Dependent Scattering Kernel," *Ann. Nucl. Energy*, **36**, 470 (2009).

10. T. Misawa, H. Unesaki, C. H. Pyeon, *Nuclear Reactor Physics Experiments*, Kyoto University Press (2010).

11. H. J. Shim, B. S. Han, J. S. Jung, H. J. Park, C. H. Kim, "McCARD: Monte Carlo Code for Advanced Reactor Design and Analysis,"

Nucl. Eng. Technol., **44**[2], 161 (2012).

12. M. Mori, S. Shiroya, K. Kanda, "Temperature Coefficient of Reactivity in Light-Water Moderated and Reflected Cores Loaded with Highly-Enriched-Uranium Fuel," *J. Nucl. Sci. Technol.*, **24**[8], 653 (1987).

13. S. Shiroya, K. Kanda, K. Tsuchihashi, "Analyses of Reactor Physics Experiments in the Kyoto University Critical Assembly," *Nucl. Sci. Eng.*, **100**, 525 (1988).

14. T. B. Fowler, D. R. Vondy, G. W. Cunningham, "Nuclear Reactor Core Analysis Code: CITATION," ORNL-TM-2496, Oak Ridge National Laboratory (1969).

15. K. Tsuchihashi et al., "Revised SRAC Code System," JAERI 1302, Japan Atomic Energy Research Institute (1986).

16. F. B. Brown, W. R. Martin, Y. Gokhan, S. Wilderman, "Progress with On-The-Fly Neutron Doppler Broadening in MCNP," LA-UR-12-22277, Los Alamos National Laboratory (2012).

17. H. J. Shim, Y. Kim, C. H. Kim, "Estimation of Adjoint-Weighted

Kinetics Parameters in Monte Carlo Forward Calculations,"' Proc. Topl. Mtg. Reactor Physics (PHYSOR2010), Pittsburgh, PA, May 9-14, 2010, on CD-ROM, (2010).

18. H. Hurwitz, "Physical Interpretation of the Adjoint Flux: Iterated Fission Probability," *Naval Reactor Physics Handbook*, Vol. I, pp. 864-869, A. Radkowsky, Ed., U.S. Atomic Energy Commission (1964).

19. R. E. MacFarlane and D. W. Muir, "NJOY99.0 Code System for Producing Pointwise and Multigroup Neutron and Photon Cross Sections from ENDF/B Data," PSR-480/NJOY99.0, Los Alamos National Laboratory (2000).

초 록

본 연구는 서울대학교 연속 에너지 몬테칼로 중성자 수송해석 코드인 McCARD의 등온 반응도 계수 계산 체계 구축을 목표로 수행되었다. 교토대 임계 집합체의 경수를 감속재로 사용하는 C형 노심에서 중수 탱크를 삽입한 경우와 인출한 경우에 대해 등온 반응도 계수 측정을 위한 실험을 수행하고 실험결과는 McCARD의 전산 결과와 비교 분석되었다. 실험에서 얻어진 등온 반응도 계수는 먼저 McCARD 코드의 검증을 위해 몬테칼로 직접 차이법에 의해 계산된 등온 반응도 계수와 비교되었으며, 그 뒤 중수와 경수의 온도 변화에 따른 감속재와 반사체 영역의 냉각재의 밀도 및 미시적 핵반응 단면적의 변화가 등온 반응도 계수에 미치는 민감도를 몬테칼로 수반해 가중 섭동법을 이용해 분석했다. 특히, 몬테칼로 섭동법을 활용한 민감도 분석 과정에서 열중성자 에너지 영역에서 경수와 중수가 등온 반응도 계수에 미치는 영향을 얻기 위해 열중성자 산란 단면적 섭동을 위한 새로운 기법이 제시되었다. 몬테칼로 섭동 분석의 결과로부터 두 노심의 등온 반응도 계수는 감속재 영역의 경수의 수밀도 감소에 의한 음의 영향과 반사체 영역의 경수의 열중성자 산란 단면적의 변화에 의한 양의 효과를 합쳐 정확히 얻어짐을 입증하였으며 열중성자 산란 단면적이 교토대 임계 집합체의 C형 노심의 등온 반응도 계수에 큰 영향을 주는 것을 새롭게 제시한 방법을 통해 분석이 가능함을 보였다.

주요어:

등온 반응도 계수
교토대 임계 집합체
몬테칼로 섭동법
McCARD

학번: 2012-23285